

Crystal structure, high-pressure, and high-temperature behavior of carbonates in the $\text{K}_2\text{Mg}(\text{CO}_3)_2$ – $\text{Na}_2\text{Mg}(\text{CO}_3)_2$ join

ANASTASIA GOLUBKOVA^{1,*}, MARCO MERLINI² AND MAX W. SCHMIDT¹

¹Institute of Geochemistry and Petrology, ETH Zurich, 8092 Zurich, Switzerland

²Dipartimento di Scienze della Terra, Università degli Studi di Milano, 20133 Milano, Italy

ABSTRACT

Although alkali-alkali earth carbonates have not been reported from mantle-derived xenoliths, these carbonates may have a substantial role in mantle metasomatic processes through lowering melting temperatures. On the $\text{Na}_2\text{Mg}(\text{CO}_3)_2$ – $\text{K}_2\text{Mg}(\text{CO}_3)_2$ join only the Na-end-member eitelite ($R\bar{3}$ space group), was reported in nature. The K-end-member ($R\bar{3}m$) readily hydrates even at low temperatures, therefore, only baylissite, $\text{K}_2\text{Mg}(\text{CO}_3)_2 \cdot 4\text{H}_2\text{O}$, has been observed. Because of the role of (K,Na)Mg-double carbonates in mantle metasomatism, we performed high P - T experiments on $\text{K}_2\text{Mg}(\text{CO}_3)_2$, $(\text{K}_{1.1}\text{Na}_{0.9})_2\text{Mg}(\text{CO}_3)_2$, and $\text{Na}_2\text{Mg}(\text{CO}_3)_2$. Structure refinements were done upon compression of single crystals from 0 to 9 GPa at ambient temperature employing synchrotron radiation. Fitting the compression data to the second-order Birch-Murnaghan EoS resulted in $V_0 = 396.2(4)$, $381.2(5)$, and $347.1(3) \text{ \AA}^3$ and $K_0 = 57.0(10)$, $54.9(13)$, and $68.6(13) \text{ GPa}$ for $\text{K}_2\text{Mg}(\text{CO}_3)_2$, $(\text{K}_{1.1}\text{Na}_{0.9})_2\text{Mg}(\text{CO}_3)_2$, and $\text{Na}_2\text{Mg}(\text{CO}_3)_2$, respectively. These compressibilities are lower than those of magnesite and dolomite. The KMg-double carbonate transforms into a monoclinic polymorph at 8.05 GPa; the high- P phase is 1% denser than the low- P polymorph. The NaMg-double carbonate has a phase transition at $\sim 14 \text{ GPa}$, but poor recrystallization has prevented structure refinement. The parameters for a V - T EoS were collected at 25–600 °C and ambient pressure and are $\alpha_0 = 14.31(5) \times 10^{-5} \text{ K}^{-1}$ and $16.73(11) \times 10^{-5} \text{ K}^{-1}$ for $\text{K}_2\text{Mg}(\text{CO}_3)_2$ and $\text{Na}_2\text{Mg}(\text{CO}_3)_2$, respectively. Moreover, fitting revealed an anisotropy of thermal expansion along the a - and c -axis: $\alpha_0(a) = 2.84(6) \times 10^{-5}$ and $4.78(5) \times 10^{-5} \text{ K}^{-1}$ and $\alpha_0(c) = 10.47(11) \times 10^{-5}$ and $8.72(5) \times 10^{-5} \text{ K}^{-1}$ for $\text{K}_2\text{Mg}(\text{CO}_3)_2$ and $\text{Na}_2\text{Mg}(\text{CO}_3)_2$, respectively.

Keywords: Alkali-alkali earth double carbonates, synchrotron, high pressure, phase transition

INTRODUCTION

Eitelite, $\text{Na}_2\text{Mg}(\text{CO}_3)_2$, represents the sodium end-member for carbonates on the $\text{K}_2\text{Mg}(\text{CO}_3)_2$ – $\text{Na}_2\text{Mg}(\text{CO}_3)_2$ join. The potassium end-member, $\text{K}_2\text{Mg}(\text{CO}_3)_2$, readily hydrates even at ambient temperatures, therefore, only baylissite, $\text{K}_2\text{Mg}(\text{CO}_3)_2 \cdot 4\text{H}_2\text{O}$, was observed in nature (Bucat et al. 1977). Nevertheless, alkali-bearing carbonates may have a substantial role in petrological processes relevant to metasomatism and melting of the Earth's mantle, because they lower mantle melting temperatures (Brey et al. 2011; Ghosh et al. 2009; Gasparik and Litvin 2002), which in turn influences the generation of deeply seated magmas. The most pronounced effect on the depression of the peridotite solidus was observed in systems containing K_2O and CO_2 (Brey et al. 2011; Ghosh et al. 2009). The decrease in melting temperatures can reach $\sim 600 \text{ °C}$ relative to dry peridotites (Brey et al. 2011; Hirschmann 2000), resulting in a solidus ~ 150 – 370 °C below the mantle geotherm (Brey et al. 2008). In fact, the melting relations in K- and CO_2 -rich peridotites are largely governed by the thermal stabilities of carbonates (Golubkova and Schmidt 2015).

A renewed interest in alkali carbonates is documented by experimental studies on phase relations in the K–Na–Mg–Ca carbonate system at high P - T conditions (e.g., Shatskiy et al. 2013a, 2013b), but detailed investigations of crystallochemical

properties of this solid solution are lacking. In this study, we report synthesis, a crystallochemical characterization, high-pressure single-crystal structure refinements and X-ray powder diffraction experiments at high temperature of alkali-bearing carbonates on the $\text{K}_2\text{Mg}(\text{CO}_3)_2$ – $\text{Na}_2\text{Mg}(\text{CO}_3)_2$ join. Parameters for a P - V equation of state (EoS) were derived from data at 0–9 GPa at ambient temperature and parameters for a V - T equation of state from data at 25–600 °C at ambient pressure. Following the report on a possible phase transition at 6.5 GPa and 1000 °C in $\text{K}_2\text{Mg}(\text{CO}_3)_2$ (Shatskiy et al. 2013b), we performed ambient temperature single-crystal experiments up to 19 GPa for the potassium end-member.

Carbonates as possible alkali hosts in the Earth's mantle

According to geochemical estimates, alkali abundances in the Earth's mantle are 2590 and 260 ppm for Na and K, respectively (Palme and O'Neill 2003). In a mantle, unaffected by metasomatic processes, alkalis are hosted in silicate structures as solid-solution in relatively low concentrations, but may be also incorporated in carbonates. Alkali-bearing carbonates in mantle-derived material are rare, although they are expected to play a geochemical role (e.g., Golubkova and Schmidt 2015; Brey et al. 2011). Giuliani et al. (2012) reported a wide range of K–Na–Ca–Mg carbonate inclusions found in metasomatic ilmenites originating from $\sim 3.5 \text{ GPa}$. These carbonates include gregoryite, $(\text{Na}_2\text{K}_2\text{Ca})\text{CO}_3$, nahcolite, NaHCO_3 , natrite, Na_2CO_3 ,

* E-mail: nastya.golubkova@gmail.com

fairchildite, $K_2Ca(CO_3)_2$, nyerereite/shortite, $Na_2Ca(CO_3)_2$, and eitelite, $Na_2Mg(CO_3)_2$. Furthermore, the presence of C in its oxidized form in association with alkalis at depth is documented by alkali-bearing Mg-rich carbonate fluid inclusions in diamonds (Klein-BenDavid et al. 2009; Zedgenizov et al. 2009).

To enable (K,Na)Mg-double carbonates in the mantle, particular redox, thermal, and compositional requirements need to be met. The stabilization of carbonates takes place at oxygen fugacities close to the C (diamond/graphite)– CO_2/CO (CCO) equilibrium, which mantle equivalent is the enstatite–magnetite–olivine–graphite/diamond (EMOG/D) buffer. The latter lies approximately 3.5 log units above the iron–wüstite (IW) buffer along cratonic geotherms (Frost and McCammon 2008), and most of the Earth's mantle at depths greater than 250 km is thought to be buffered close to IW. Hence, only somewhat oxidized mantle zones would host carbonates. Taking into account average abundances of alkalis and C in the primitive mantle, the appearance of alkali- and, particularly, KMg-double carbonates requires enrichment of mantle peridotites, possible through metasomatism by alkali-rich carbonate melts. Such melts can be generated during the subduction of carbonated metapelites, which K_2O/Na_2O wt-ratios vary with pressure, at 5–16 GPa carbonate melts with $K_2O/Na_2O > 1$ result (Grassi and Schmidt 2011a, 2011b).

The thermal stability of (K,Na)Mg-double carbonates should be confined to relatively cold and by implication shallow mantle regions. The melting of $K_2Mg(CO_3)_2$ – $Na_2Mg(CO_3)_2$ carbonates has not been studied over a wide *P-T* range. Experiments at 6 and 8 GPa indicate that in presence of H_2O KMg- and NaMg-double carbonates melt out between 900–1000 and 1000–1100 °C, respectively (Shatskiy et al. 2013a, 2013b). Such low temperatures are consistent with the experiments on H_2O -bearing peridotite+carbonatite systems (Golubkova and Schmidt 2015), where $K_2Mg(CO_3)_2$ melts out at 900 °C, 8 GPa. The maximum depth of the thermal stability of (K,Na)Mg-double carbonates can be estimated if a cold cratonic geotherm is considered (40 mW/m², Artemieva 2009; Pollack and Chapman 1977); along such a geotherm, the 900–1100 °C range corresponds to 120–170 km depths.

Structural characteristics of (K,Na)Mg-double carbonates at ambient conditions

There is no systematic study on the structural behavior and thermo-elastic properties of (K,Na)Mg-double carbonates. Table 1 reports known alkali-alkaline earth carbonates, some of them occurring as minerals. From this list, $K_2Mg(CO_3)_2$ and high-*T* nyerereite have never been found in nature. Gregoryite and nyerereite crystals were reported in the natro-carbonatite

lavas of the Oldoinyo Lengai volcano, Tanzania (e.g., McKie and Frankis 1977; Dawson 1962a, 1962b), whereas the first findings of eitelite, buetschliite, and fairchildite were not magmatic occurrences (e.g., Pertlik 1981; Pabst 1974, 1973).

At atmospheric pressure $K_2Mg(CO_3)_2$ crystallizes in a trigonal $R\bar{3}m$ space group and is isostructural to buetschliite (Hesse and Simons 1982). Eitelite, $Na_2Mg(CO_3)_2$, on the contrary, crystallizes with $R\bar{3}$ symmetry (Pabst 1974). The topologies of buetschliite and eitelite are similar, but different orientations of the carbonate groups and different coordination polyhedra of the alkali metals lead to the presence or absence of a mirror plane. The structure of alkali-Mg-double carbonates can be described by alternating layers of divalent cations and alkali cations, separated by parallel oriented triangular carbonate groups. The number of divalent cations is half that of alkali metals, to keep electrostatic balance. The Mg atoms feature a [6]-fold octahedral coordination. They are connected through CO_3 groups, with different geometries resulting in $R\bar{3}m$ and $R\bar{3}$ structures (Fig. 1). In $K_2Mg(CO_3)_2$ the potassium atom is bonded to 9 near neighbor O atoms, with 6 shorter bonds of same distance and three longer ones (Fig. 1a). In eitelite, $Na_2Mg(CO_3)_2$, Na is still in ninefold coordination, but the six shorter Na–O bonds are no longer equivalent, and present two groups of distances (Fig. 1b). The Na coordination polyhedron is more distorted, which can be ascribed to the smaller ionic size compared to potassium. The structural similarity indicates that eitelite and buetschliite can incorporate significant amounts of $K_2Mg(CO_3)_2$ component.

EXPERIMENTAL METHODS

Sample preparation

For structure refinements we used single crystals of (K,Na)Mg-double carbonates, synthesized in piston cylinders at ETH Zurich. For synthesis, powders of natural magnesite ($Mg_{0.998}Fe_{0.002}CO_3$, Brazil) and synthetic alkali carbonates (K_2CO_3 and Na_2CO_3) were mixed in the desired molar proportions to obtain carbonates of composition: $K_2Mg(CO_3)_2$, $K_{1.1}Na_{0.9}Mg(CO_3)_2$, and $Na_2Mg(CO_3)_2$. Because of the hygroscopic nature of alkali carbonates, starting mixtures were kept for 10–12 h in a 220 °C oven before loading into Au capsules. To perform experiments at 2 GPa, a NaCl–pyrex–graphite–MgO assembly was employed. Run temperatures were 500 °C for $K_2Mg(CO_3)_2$ and 600 °C for $Na_2Mg(CO_3)_2$ and $(K,Na)_2Mg(CO_3)_2$. Phase relations in the K_2CO_3 – Na_2CO_3 – $MgCO_3$ systems are not known at the conditions of our experiments, nevertheless, the absence of quenched liquid in recovered charges indicates that experimental pressures and temperatures corresponded to subsolidus conditions. To enhance equilibration and growth of relatively large single crystals, run times were 4–5 days. Experimental products were analyzed with a JEOL JSM6300 field emission SEM with EDS detector; for carbonate analyses areas of $5\text{--}10 \times 5\text{--}10 \mu\text{m}$ were scanned to prevent alkali losses. The average composition of the intermediate compound is $K_{1.1}Na_{0.9}Mg(CO_3)_2$ (with standard deviation is listed in Table 2).

TABLE 1. Alkali-alkaline earth double carbonates and their structural characteristics

Formula	Mineral name	Remark	Space group	<i>a</i> (Å)	<i>b</i> (Å)	<i>c</i> (Å)	Z	Reference
$Na_2Mg(CO_3)_2$	Eitelite		$R\bar{3}$	4.942		16.406	3	(Pabst 1973)
$(Na,K)_2Ca(CO_3)_2^a$	Nyerereite	Low- <i>T</i>	$Cmc2_1$	5.044	8.809	12.743	4	(McKie and Frankis 1977)
$(Na,K)_2Ca(CO_3)_2$		High- <i>T</i>	$P6_3mc$	5.05		12.85	2	(McKie and Frankis 1977)
$Na_2Ca_2(CO_3)_3$	Shortite		$Amm2$	4.961	11.03	7.12	2	(Gaines et al. 1997)
$(Na_2,K_2)CaCO_3$	Gregoryite		$P6_3mc$	5.215		6.584	2	(Anthony et al. 1997)
$K_2Ca(CO_3)_2^b$	Buetschliite	Low- <i>T</i>	$R\bar{3}m$	5.38		18.12	3	(Pabst 1974)
$K_2Ca(CO_3)_2^b$	Fairchildite	High- <i>T</i>	$P6_3/mmc$	5.294		13.355	2	(Pertlik 1981)
$K_2Ca(CO_3)_2$			$R\bar{3}$	13.010		8.615	6	(Winbo et al. 1997)
$K_2Mg(CO_3)_2$			$R\bar{3}m$	5.15		17.29	3	(Hesse and Simons 1982)

^a Natural nyerereite represents an inversion from a high-*T* hexagonal polymorph (McKie and Frankis 1977).

^b The transition temperature between buetschliite and fairchildite is suggested to be in the range 505–585 °C (Pabst 1974).

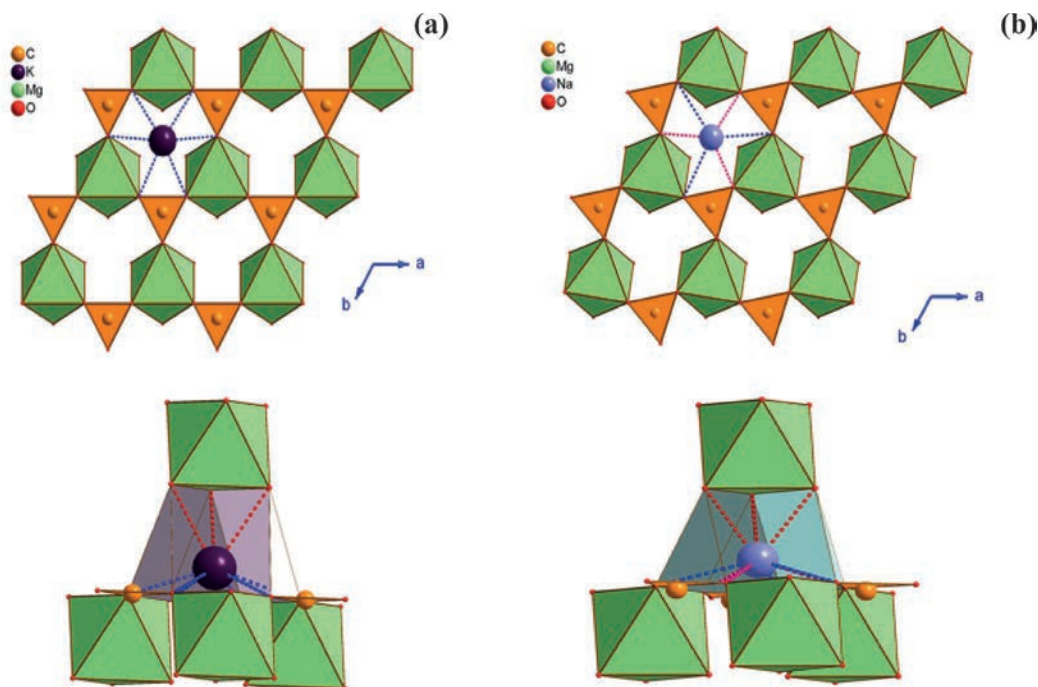


FIGURE 1. Crystal structures of (a) $\text{K}_2\text{Mg}(\text{CO}_3)_2$ (low-pressure polymorph) and (b) $\text{Na}_2\text{Mg}(\text{CO}_3)_2$.

Synchrotron X-ray single-crystal diffraction

In situ high-pressure synchrotron X-ray single-crystal diffraction was performed at the beamline ID09 of the European Synchrotron Radiation Facility, ESRF (Grenoble, France). The standard beamline set up was used (Merlini and Hanfland 2013), employing a Mar555 detector and a monochromatic beam with a wavelength of $\lambda = 0.41272(6)$ Å with a spot size of $30 \times 30 \mu\text{m}^2$ on the sample. To study compressibility at room temperature, samples were placed into the experimental chamber of the diamond-anvil cell (DAC) with a pair of beveled diamonds (600 μm culet diameter) and a steel gasket. In the experiments with $\text{K}_{1.1}\text{Na}_{0.9}\text{Mg}(\text{CO}_3)_2$ and $\text{Na}_2\text{Mg}(\text{CO}_3)_2$ an ethanol-methanol mixture was used as pressure-transmitting medium, enabling hydrostatic conditions over the studied pressure range. The compressibility of single crystals of $\text{K}_{1.1}\text{Na}_{0.9}\text{Mg}(\text{CO}_3)_2$ and $\text{Na}_2\text{Mg}(\text{CO}_3)_2$ was studied from ambient pressure to 8 GPa, 10–12 data points were collected for each phase (Tables 3–4). The determination of possible phase transitions and compressibility measurements for $\text{K}_2\text{Mg}(\text{CO}_3)_2$ were done over a wider pressure range to 19 GPa (Tables 5a–5d). Therefore, helium gas was employed in these experiments as a pressure-transmitting medium assuring hydrostatic pressure. Experimental pressures were determined based on the shift of the fluorescence peaks in ruby. A phase transition of $\text{K}_2\text{Mg}(\text{CO}_3)_2$ carbonate was observed between 8.05 and 9.47 GPa and further on we will refer to the lower-pressure polymorph as $\text{K}_2\text{Mg}(\text{CO}_3)_2$ -I and to the higher-pressure phase as $\text{K}_2\text{Mg}(\text{CO}_3)_2$ -II. Single-crystal diffraction data were integrated with the CrysAlis software (Oxford Diffraction) and structure solution and refinement were performed with the Jana2006 (Petríček et al. 2014) and Superflip (Palatinus and Chapuis 2007) software packages.

High-temperature powder diffraction data were collected at the MCX beamline of the Elettra Synchrotron (Trieste, Italy). For the $\text{Na}_2\text{Mg}(\text{CO}_3)_2$ sample, we used the high-resolution diffractometer available at the beamline equipped with a gas-blower furnace. Calibration with thermal expansion and the phase transitions of standard quartz indicate a precision of 2 °C in temperature. For the $\text{K}_2\text{Mg}(\text{CO}_3)_2$ sample, we observed a rapid hydration and decomposition of the sample, therefore we used a furnace (Riello et al. 2013) equipped with a translating imaging plate, which allows a controlled atmosphere and rapid data acquisition. For our purpose we used 1.5 bar P_{CO_2} . The CO_2 atmosphere and the whole data collection time, approximately 1 h for the whole experiment, allowed collection of data up to 400 °C. In this case temperature accuracy is in the order of 5 °C. Samples were loaded into quartz glass capillaries and heated up to 400 °C [$\text{K}_2\text{Mg}(\text{CO}_3)_2$] and 500 °C [$\text{Na}_2\text{Mg}(\text{CO}_3)_2$] (Table 6). The wavelength of the monochromatic beam employed in these experiments was $\lambda = 0.82618$ Å. X-ray powder patterns were fitted with

TABLE 2. Chemical composition of $\text{K}_{1.1}\text{Na}_{0.9}\text{Mg}(\text{CO}_3)_2$ (EDS analysis)

wt%	$n = 5$
Na ₂ O	13.6(2)
K ₂ O	25.8(2)
MgO	18.6(0)
CO ₂	42.0 ^a
apfu (5 cations)	
Na	0.91(1)
K	1.14(1)
Mg	0.96(0)
C	5.00 ^a

Notes: Average composition of 5 scanned areas; numbers in parentheses are 1 σ standard deviations.

^a Calculated from stoichiometry.

the Rietveld method using the GSAS-ExpGui software (Toby 2001; Larson and Von Dreele 1994).

RESULTS

Structural variations depending on composition

Structure refinements indicate that at room pressure and temperature $\text{K}_2\text{Mg}(\text{CO}_3)_2$ crystallizes in $R\bar{3}m$ space group, whereas $\text{Na}_2\text{Mg}(\text{CO}_3)_2$ in $R\bar{3}$, which is consistent with the published data for KMg- and NaMg-double carbonates (Hesse and Simons 1982; Pabst 1973). $\text{K}_{1.1}\text{Na}_{0.9}\text{Mg}(\text{CO}_3)_2$ presents the same symmetry as the pure K-end-member ($R\bar{3}m$). Unit-cell parameters (a and c) of the three different carbonates exhibit an almost linear dependence with V ($R^2 = 1.0$) and vary almost linearly between $\text{K}_2\text{Mg}(\text{CO}_3)_2$ and $\text{Na}_2\text{Mg}(\text{CO}_3)_2$. The volume decrease from the K- to Na-end-member is almost 13%, whereas the decrease in the a - and c -axes is 4 and 5%, respectively. These carbonate structures are comprised of $[\text{MgO}_6]$ -octahedra, $[(\text{K},\text{Na})\text{O}_9]$ -polyhedra, and $[\text{CO}_3]^{2-}$ -groups. Interatomic distances decrease with substitution of K by Na. The six Mg–O distances are equivalent for all studied carbon-

TABLE 3. Variation of lattice parameters, interatomic distances, and O–C–O angle with P for $(K_{1.1}Na_{0.9})_{\Sigma 2}Mg(CO_3)_2$

P (GPa)	a (Å)	c (Å)	V (Å ³)	K,Na1–O1 (Å) 6 \times	K,Na1–O1 (Å) 3 \times	Mg1–O1 (Å) 6 \times	C1–O1 (Å) 3 \times	O1–C1–O1 3 \times
0.01(1)	5.088(1)	17.022(6)	381.7(5)	2.679	2.876	2.080	1.279	119.94
0.32(1)	5.084(1)	16.923(2)	378.7(5)	2.670	2.833	2.100	1.272	119.84
0.87(1)	5.080(1)	16.828(2)	376.0(5)	2.676	2.834	2.067	1.283	119.78
1.81(1)	5.062(1)	16.619(2)	368.7(5)	2.654	2.801	2.068	1.276	119.75
2.39(1)	5.063(1)	16.538(2)	367.2(5)	2.657	2.796	2.059	1.275	119.91
3.03(1)	5.040(1)	16.379(2)	360.3(5)	2.648	2.781	2.033	1.275	119.99
4.01(1)	5.038(1)	16.265(2)	357.5(5)	2.643	2.753	2.049	1.274	119.97
5.05(1)	5.023(1)	16.117(2)	352.1(5)	2.630	2.729	2.026	1.274	120.00
6.04(1)	5.015(1)	16.005(2)	348.7(5)	2.622	2.702	2.031	1.270	119.98
6.78(1)	5.006(1)	15.902(2)	345.1(5)	2.620	2.702	2.017	1.266	119.97
7.56(1)	4.996(1)	15.798(2)	341.5(5)	2.607	2.686	2.010	1.270	119.95
8.20(1)	4.987(1)	15.731(2)	338.7(5)	2.597	2.661	2.010	1.273	119.92

Note: Values in parentheses represent 1 σ errors.**TABLE 4.** Variation of lattice parameters, interatomic distances, and O–C–O angle with P for $Na_2Mg(CO_3)_2$

P (GPa)	a (Å)	c (Å)	V (Å ³)	Na1–O1 (Å) 3 \times	Na1–O1 (Å) 3 \times	Na1–O1 (Å) 3 \times	Mg1–O1 (Å) 6 \times	C1–O1 (Å) 3 \times	O1–C1–O1 3 \times
0	4.939(1)	16.382(10)	346.0(4)	2.607(5)	2.938(3)	2.341(3)	2.077(4)	1.282(5)	120.0(3)
0.29(1)	4.939(1)	16.368(10)	345.8(4)						
0.92(1)	4.928(1)	16.281(10)	342.5(4)	2.608(5)	2.936(3)	2.335(3)	2.076(5)	1.281(5)	120.0(4)
1.23(1)	4.924(1)	16.217(10)	340.5(4)						
1.84(1)	4.914(1)	16.176(10)	338.2(4)						
2.88(1)	4.900(1)	16.069(10)	334.1(4)						
3.74(1)	4.887(1)	15.966(10)	330.2(4)						
4.85(1)	4.873(1)	15.857(10)	326.0(4)						
5.95(1)	4.860(1)	15.757(10)	322.3(4)						
5.95(1)	4.858(1)	15.764(10)	322.2(4)	2.485(5)	2.927(3)	2.272(3)	2.032(5)	1.277(5)	120.0(4)
0*	4.9514(3)	16.425(3)	348.7(3)						
8.03(1)*	4.8437(3)	15.616(5)	317.3(3)						
8.68(1)*	4.8367(3)	15.562(5)	315.3(3)						
9.65(1)*	4.8276(4)	15.492(6)	312.7(3)						
11.37(1)*	4.8082(6)	15.372(10)	307.8(3)						
12.52(1)*	4.7973(5)	15.294(9)	304.8(3)						
13.66(1)*	4.7872(4)	15.212(7)	301.9(2)						
	a (Å)	b (Å)	c (Å)	α (°)	β (°)	γ (°)	V (Å ³)		
15.29(1)	8.29(5)	4.839(18)	5.65(3)	88.3(4)	118.1(6)	90.4(4)	200(2)		
16.70(1)	8.34(2)	4.761(7)	5.548(15)	89.39(16)	118.0(3)	89.47(15)	194.4(8)		

Notes: Values in parentheses represent 1 σ errors; structure refinements were done at 0, 0.92, and 5.95 GPa. * indicates a second run at pressures >6 GPa.**TABLE 5a.** Variation of lattice parameters, interatomic distances, and O–C–O angle with P for $K_2Mg(CO_3)_2$ -I

P (GPa)	a (Å)	c (Å)	V (Å ³)	K1–O1 (Å) 6 \times	K1–O1 (Å) 3 \times	Mg1–O1 (Å) 6 \times	C1–O1 (Å) 3 \times	O1–C1–O1 3 \times
0.0	5.154(1)	17.288(1)	397.7(4)	2.731(4)	2.928(6)	2.096(4)	1.288(3)	119.96(14)
0.13(10)	5.149(1)	17.261(1)	396.4(4)	2.731(4)	2.923(6)	2.097(4)	1.283(3)	119.95(14)
0.49(10)	5.144(1)	17.144(1)	392.8(4)	2.725(4)	2.906(6)	2.091(4)	1.283(3)	119.96(14)
1.00(10)	5.136(1)	17.038(1)	389.3(4)	2.716(4)	2.888(6)	2.087(4)	1.283(3)	119.94(16)
1.59(10)	5.131(1)	16.942(1)	386.2(4)	2.711(4)	2.868(6)	2.087(4)	1.280(3)	119.90(16)
2.31(10)	5.120(1)	16.796(1)	381.4(4)	2.670(4)	2.850(6)	2.074(4)	1.285(3)	119.96(16)
3.09(10)	5.111(1)	16.636(1)	376.3(4)	2.691(4)	2.823(7)	2.066(4)	1.285(3)	119.97(16)
4.01(10)	5.103(1)	16.473(1)	371.5(4)	2.684(4)	2.810(7)	2.061(4)	1.278(3)	119.98(16)
5.06(10)	5.093(1)	16.320(1)	366.6(4)	2.674(4)	2.793(7)	2.045(4)	1.285(3)	119.97(16)
6.03(10)	5.088(1)	16.202(1)	363.2(4)	2.666(4)	2.772(7)	2.042(4)	1.285(3)	119.99(16)
7.04(10)	5.076(1)	16.068(1)	358.5(4)	2.658(4)	2.764(7)	2.036(4)	1.277(3)	119.98(16)
4.76(10)	5.0978(1)	16.381(1)	368.7(4)					
0.10(10)	5.1513(1)	17.262(1)	396.7(4)					

Note: Values in parentheses represent 1 σ errors.

ates and vary from 2.096 to 2.077 Å between $K_2Mg(CO_3)_2$ and $Na_2Mg(CO_3)_2$. The interatomic distances between alkali cations and oxygen atoms shorten from the K- to the Na-end-member. The distances between C and O atoms and O–C–O angles are equal since the C atoms are located on the threefold axes. There is no linear variation between the C–O distances, O–C–O angles and composition (Tables 3–5). The lengths of C–O interatomic bonds and angles equal 1.288(2), 1.279(6), and 1.282(4) Å and 119.96(14), 119.94(16), and 119.98(14)° for $K_2Mg(CO_3)_2$ -I, $K_{1.1}Na_{0.9}Mg(CO_3)_2$, and $Na_2Mg(CO_3)_2$, respectively.

Phase behavior upon compression

In the following section we describe the results of fitting the compressibility data to a P - V EoS and of the pressure-induced phase transition of $K_2Mg(CO_3)_2$. EoS parameters were defined for both low- and high- P $K_2Mg(CO_3)_2$ polymorphs. The structure refinement was also done for $K_2Mg(CO_3)_2$ -II and a detailed structure description is provided in the subsequent section.

Defining the parameters of the P - V equation of state. The variation of the unit-cell parameters and interatomic distances with P are listed in Tables 3–5 and shown in Figures 2a–2e. The

volume-pressure data were fitted to the second-order Birch-Murnaghan EoS. Calculation of the “normalized stresses” and plotting these values against the Eulerian finite strain indicated that the truncation to the second-order Birch-Murnaghan EoS with K' fixed at 4 is appropriate to describe the observed *P-V* behavior (Angel 2000). Fit results for the studied carbonates are presented in Table 7.

All studied carbonates are characterized by a higher compressibility along the *c*- than *a*-axis (Figs. 2a and 2b), similarly, the bonds in [K₂O₆]- or [NaO₆]-polyhedra are more compressible than in [MgO₆]-octahedra (Figs. 2d–2e). Figure 3 and Table 7 demonstrate the variation of K_0 with composition. On the K₂Mg(CO₃)₂–Na₂(CO₃)₂ join carbonates are characterized by an increase in bulk modulus with substitution of Na by K. The anisotropy of compression is stronger in KMg- (low-*P* polymorph) and (K,Na)Mg-double carbonates than in the NaMg-end-member: to 6 GPa, the shortening of the *a*-axis was 1.4, 2.0, and 1.6% for KMg-, (K,Na)Mg-, and NaMg-double carbonates, respectively, whereas shortening along the *c*-axis was 6.3, 7.6, and 3.8% for KMg-, (K,Na)Mg-, and NaMg-double carbonates, respectively.

K₂Mg(CO₃)₂ phase transition and the structure of K₂Mg(CO₃)₂-II. Pressure increase to 8.05 GPa resulted in the transformation of K₂Mg(CO₃)₂-I into the K₂Mg(CO₃)₂-II polymorph. Figure 4 shows volume per formula unit changes upon compression of K₂Mg(CO₃)₂. Any attempt to index diffraction peaks collected at 9.47 GPa with a rhombohedral unit cell, using the orientation matrix from the previous pressure point, resulted in a distorted hexagonal lattice, with α and β angles significantly deviating from 90° (unit-cell parameters: $a = 5.050$ Å, $b = 5.047$ Å, $c = 15.928$ Å, $\alpha = 86.94^\circ$, $\gamma = 93.09^\circ$, $\beta = 119.71^\circ$).

TABLE 5b. Variation of lattice parameters with *P* for K₂Mg(CO₃)₂-II

<i>P</i> (GPa)	<i>a</i> (Å)	<i>b</i> (Å)	<i>c</i> (Å)	β	<i>V</i> (Å ³)
8.05(10)	8.753(5)	5.0669(7)	6.238(8)	121.69(13)	235.4(2)
9.47(10)	8.718(3)	5.058(1)	6.229(1)	122.55(16)	231.5(4)
9.81(10)	8.712(3)	5.055(1)	6.229(1)	122.74(16)	230.8(4)
10.78(10)	8.695(3)	5.046(1)	6.219(1)	123.18(16)	228.4(4)
11.94(10)	8.667(3)	5.039(1)	6.210(1)	123.63(16)	225.8(4)
13.00(10)	8.647(3)	5.030(1)	6.199(1)	124.01(16)	223.5(4)
14.15(10)	8.626(3)	5.021(1)	6.185(1)	124.41(16)	221.0(4)
15.26(10)	8.595(3)	5.010(1)	6.176(1)	124.80(16)	218.4(4)
16.20(10)	8.590(3)	5.004(1)	6.159(1)	124.92(16)	217.1(4)
17.14(10)	8.574(3)	4.997(1)	6.149(1)	125.13(16)	215.5(4)
18.17(10)	8.560(3)	4.990(1)	6.139(1)	125.32(16)	214.0(4)
18.96(10)	8.551(3)	4.984(1)	6.127(1)	125.47(16)	212.7(4)
10.08(10)	8.712(3)	5.058(1)	6.228(1)	122.72(16)	230.9(4)

Note: Values in parentheses represent 1 σ errors.

This lattice, transformed in a conventional unit cell, results in a *C*-centered monoclinic lattice with the following parameters: $a = 8.753(5)$, $b = 5.0669(7)$, $c = 6.238(8)$ Å, $\alpha = \gamma = 90.0^\circ$, $\beta = 121.69(13)^\circ$. A careful analysis of the diffraction peaks indicates the presence of two twin domains, which can be derived from the low-pressure rhombohedral cell (in the hexagonal setting) with the application of the following transformation matrixes: $(-1\ 1\ 0; 1\ 1\ 0; \frac{1}{3}\ -\frac{1}{3}\ -\frac{1}{3})$ for the first twin domain, and $(1\ 2\ 0; -1\ 0\ 0; -\frac{1}{3}\ -\frac{2}{3}\ \frac{1}{3})$ for the second domain. Structure solution and refinements were performed using the integrated data from one domain. The correctness of the *C*-centered monoclinic lattice is demonstrated by the successful crystal structure solution,

TABLE 5d. Atomic coordinates and their variation with *P* for K₂Mg(CO₃)₂-II

		K1	Mg1	O1	O2	C1	<i>R</i> _{Bragg} %
8.05(10)	x/a	0.7864(7)	½	0.765(2)	0.4690(16)	0.399(3)	7.02
	y/b	0	–½	–½	0.2201(13)	0	
	z/c	0.362(2)	0	0.261(7)	0.200(4)	0.201(9)	
9.47(10)	x/a	0.7863(3)	½	0.7688(9)	0.4660(7)	0.4025(13)	5.64
	y/b	0	–½	–½	0.2186(6)	0	
	z/c	0.3625(4)	0	0.2570(15)	0.2044(12)	0.223(2)	
9.81(10)	x/a	0.7863(2)	½	0.7716(7)	0.4651(6)	0.4013(11)	4.35
	y/b	0	–½	–½	0.2196(5)	0	
	z/c	0.3620(3)	0	0.2602(12)	0.2031(8)	0.2205(16)	
10.78(10)	x/a	0.7864(4)	½	0.7704(12)	0.4643(9)	0.3992(16)	6.42
	y/b	0	–½	–½	0.2205(10)	0	
	z/c	0.3615(6)	0	0.262(2)	0.2006(14)	0.219(3)	
11.94(10)	x/a	0.7861(2)	½	0.7730(8)	0.4621(6)	0.4009(11)	5.15
	y/b	0	–½	–½	0.2202(6)	0	
	z/c	0.3604(4)	0	0.2677(13)	0.1980(9)	0.2213(17)	
13.00(10)	x/a	0.7858(2)	½	0.7730(6)	0.4623(5)	0.4012(12)	4.58
	y/b	0	–½	–½	0.2203(5)	0	
	z/c	0.3597(3)	0	0.2682(11)	0.1982(7)	0.222(2)	
14.15(10)	x/a	0.7859(2)	½	0.7755(7)	0.4607(7)	0.4003(9)	4.62
	y/b	0	–½	–½	0.2215(5)	0	
	z/c	0.3595(3)	0	0.2738(11)	0.1961(8)	0.2205(15)	
15.26(10)	x/a	0.7856(1)	½	0.7758(5)	0.4606(4)	0.4008(7)	3.14
	y/b	0	–½	–½	0.2215(4)	0	
	z/c	0.3586(2)	0	0.2748(8)	0.1962(6)	0.2210(11)	
16.20(10)	x/a	0.78567(18)	½	0.7771(6)	0.4601(4)	0.4008(8)	3.76
	y/b	0	–½	–½	0.2215(5)	0	
	z/c	0.3582(3)	0	0.2776(10)	0.1950(7)	0.2222(13)	
17.14(10)	x/a	0.78578(19)	½	0.7777(6)	0.4600(4)	0.4007(8)	3.64
	y/b	0	–½	–½	0.2224(5)	0	
	z/c	0.3581(3)	0	0.2788(10)	0.1947(7)	0.2216(13)	
18.17(10)	x/a	0.7855(2)	½	0.7775(7)	0.4596(5)	0.4022(9)	4.02
	y/b	0	–½	–½	0.2217(5)	0	
	z/c	0.3574(3)	0	0.2794(11)	0.1944(8)	0.2237(15)	
18.96(10)	x/a	0.7852(3)	½	0.7781(10)	0.4591(7)	0.4016(14)	5.98
	y/b	0	–½	–½	0.2215(7)	0	
	z/c	0.3572(5)	0	0.2808(16)	0.1947(11)	0.224(2)	
10.08(10)	x/a	0.7864(2)	½	0.7700(7)	0.4641(5)	0.4011(9)	4.32
	y/b	0	–½	–½	0.2197(5)	0	
	z/c	0.3620(4)	0	0.2601(13)	0.2009(9)	0.2200(16)	

TABLE 5c. Variation of interatomic distances and O–C–O angle with *P* for K₂Mg(CO₃)₂-II

<i>P</i> (GPa)	K1–O1 (Å) 2x	K1–O1 (Å) 1x	K1–O2 (Å) 2x	K1–O2 (Å) 2x	K1–O2 (Å) 2x	Mg1–O1 (Å) 2x	Mg1–O2 (Å) 4x	C1–O1 (Å) 1x	C1–O2 (Å) 2x	O2–C1–O2 1x	O2–C1–O1 2x
8.05(10)	2.594(10)	2.62(4)	2.652(16)	2.70(2)	2.81(2)	2.016(18)	2.00(2)	1.41(6)	1.27(2)	122(3)	118(2)
9.47(10)	2.597(6)	2.660(12)	2.652(9)	2.667(8)	2.775(11)	2.004(11)	2.035(7)	1.293(17)	1.269(9)	121.1(12)	119.4(6)
9.81(10)	2.592(6)	2.660(10)	2.655(9)	2.661(7)	2.774(10)	2.019(10)	2.029(6)	1.272(7)	1.281(14)	121.5(10)	119.2(5)
10.78(10)	2.583(6)	2.644(15)	2.649(11)	2.660(10)	2.765(12)	1.997(12)	2.016(8)	1.282(11)	1.286(19)	120.5(15)	119.7(8)
11.94(10)	2.573(6)	2.628(11)	2.645(9)	2.653(7)	2.764(11)	2.001(11)	2.014(6)	1.291(15)	1.272(8)	121.4(10)	119.3(5)
13.00(10)	2.567(6)	2.624(10)	2.631(9)	2.649(6)	2.749(11)	1.986(10)	2.011(5)	1.290(13)	1.271(7)	121.3(9)	119.4(5)
14.15(10)	2.557(4)	2.604(10)	2.631(8)	2.641(6)	2.738(11)	1.992(10)	2.002(5)	1.292(13)	1.273(6)	121.8(9)	119.1(5)
15.26(10)	2.550(4)	2.602(8)	2.615(7)	2.634(5)	2.724(10)	1.977(9)	1.999(4)	1.293(10)	1.269(5)	122.0(6)	119.0(3)
16.20(10)	2.544(6)	2.590(9)	2.616(8)	2.631(6)	2.721(11)	1.982(10)	1.993(5)	1.289(11)	1.270(6)	121.5(8)	119.3(4)
17.14(10)	2.539(6)	2.593(9)	2.650(9)	2.661(6)	2.720(11)	1.991(10)	2.013(5)	1.312(12)	1.277(6)	121.0(8)	119.5(4)
18.17(10)	2.534(6)	2.580(9)	2.604(9)	2.622(6)	2.705(11)	1.968(11)	1.987(5)	1.295(13)	1.265(6)	122.0(8)	119.0(4)
18.96(10)	2.530(6)	2.570(13)	2.601(10)	2.617(8)	2.670(11)	1.966(12)	1.989(7)	1.290(19)	1.263(9)	122.0(13)	119.0(7)
10.08(10)	2.593(6)	2.652(10)	2.661(9)	2.663(6)	2.784(11)	2.009(10)	2.024(6)	1.294(13)	1.273(6)	121.6(9)	119.2(5)

TABLE 6. Variation of lattice parameters with T for $K_2Mg(CO_3)_2$ and $Na_2Mg(CO_3)_2$

T (°C)	$K_2Mg(CO_3)_2$			$Na_2Mg(CO_3)_2$		
	a (Å)	c (Å)	V (Å ³)	a (Å)	c (Å)	V (Å ³)
25(3)	5.155(1)	17.310(4)	398.4(2)	4.938	16.388(1)	346.1(1)
50(3)	5.157(1)	17.329(4)	399.1(2)			
75(3)	5.159(1)	17.345(4)	399.7(2)	4.943	16.417(1)	347.3(1)
100(3)	5.160(1)	17.363(4)	400.4(2)			
125(3)	5.162(1)	17.388(3)	401.3(2)	4.948	16.448(1)	348.7(1)
150(3)	5.163(1)	17.412(3)	401.9(2)			
175(3)	5.164(1)	17.436(3)	402.6(1)	4.953	16.480(1)	350.1(1)
200(3)	5.165(1)	17.458(3)	403.3(1)			
225(3)	5.166(1)	17.483(3)	404.0(1)	4.958	16.514(1)	351.5(1)
250(3)	5.167	17.500(3)	404.6(1)			
275(3)	5.169	17.523(3)	405.5(1)			
300(3)	5.170	17.547(2)	406.2(1)	4.966	16.566(1)	353.8(1)
325(3)	5.173	17.573(2)	407.2(1)			
350(3)	5.174	17.593(2)	407.8(1)	4.971	16.601(1)	355.3(1)
375(3)	5.175(1)	17.617(3)	408.6(1)			
400(3)	5.177(1)	17.635(3)	409.3(2)	4.977	16.643(1)	357.1(1)
450(3)				4.984	16.687(1)	359.0(1)
500(3)				4.991	16.727(1)	360.8(1)

Note: Values in parentheses represent 1σ errors.

achieved with the charge flipping algorithm (Oszlanyi and Suto 2007), and successive refinement with Jana2006 software resulting in a low R_{Bragg} of 3–5%. Atomic coordinates and selected interatomic distances are reported in Tables 5b–5d. The statistical agreement parameters are reported in Table 5d. $K_2Mg(CO_3)_2$ -II is monoclinic, $C2/m$, with a density of 3.14 g/cm³ at 8.05 GPa and $Z = 2$ in the unit cell. Figure 5 compares the structure of $K_2Mg(CO_3)_2$ -II with $K_2Mg(CO_3)_2$ -I. The topology is similar to the low-pressure polymorph but with a significant distortion of the structural elements. In particular, the carbonate groups are no longer parallel, but tilted. This, in turn, results in a more distorted coordination polyhedron for the alkali metal, with five different bond distances. The distortion is less pronounced for the $[MgO_6]$ -coordination polyhedron. The unit-cell volume, normalized per formula unit (V/Z), is 1% smaller than the low-pressure phase. The phase transition is reversible. In Figure 4 we also show the decompression results, which indicate that with pressure release, the high- P polymorph transforms back into the low- P structure.

$Na_2Mg(CO_3)_2$ -II above 14 GPa. Because of the similarity in structure topology between $K_2Mg(CO_3)_2$ and $Na_2Mg(CO_3)_2$, we checked a possible high-pressure transition also in the Na-end-member. A second run with $Na_2Mg(CO_3)_2$ was performed, and the single crystal was first compressed in He to 8 GPa, then pressure was increased by small steps. The rhombohedral structure was observed up to 13.6 GPa. On further pressure increase, we observed a phase transition. Unfortunately, the quality of the crystal after the transition prevents any detailed description. The diffraction peaks can be indexed with a similar unit cell as $K_2Mg(CO_3)_2$ -II, but the angles deviate from 90°. Considering that the subgroup related to the $R\bar{3}$ space group after removal of the threefold axis is only $P\bar{1}$, we may speculate that $Na_2Mg(CO_3)_2$ -II is triclinic, but the exact structure determination must still be addressed. The effect of Na seems therefore, to increase the pressure of transition, as expected on the basis of ionic radii considerations. The volume data of low-pressure $Na_2Mg(CO_3)_2$ can be fitted with a Birch-Murnaghan EoS (Table 7).

Defining the parameters of the V - T equation of state

Table 6 and Figure 6 show the data on changes in lattice parameters with increasing T . To obtain thermal expansion

coefficients, the formulation of Pawley et al. (1996), adopted by Holland and Powell (1998), was used

$$\alpha_T = \alpha_o \left(1 - \frac{10}{\sqrt{T}} \right)$$

$$V_{1,T} = V_{1,298} \left[1 + \alpha_o (T - 298) - 20\alpha_o (\sqrt{T} - \sqrt{298}) \right]$$

V_0 and α_0 obtained by fitting the V - T data are: $V_0 = 396.2(4)$ Å³, $\alpha_0 = 14.31(5) \times 10^{-5}$ K⁻¹ for $K_2Mg(CO_3)_2$ and $V_0 = 347.1(3)$ Å³, $\alpha_0 = 16.73(11) \times 10^{-5}$ K⁻¹ for $Na_2Mg(CO_3)_2$ (Table 7).

Figure 6 illustrates the relative expansions of unit-cell parameters (a/a_0 , c/c_0 , V/V_0) with increasing temperature. The NaMg-double carbonate is characterized by a larger increase in volume upon heating (4%) in comparison to the K-end-member (3%, to 400 °C). Both carbonates demonstrate anisotropy in thermal expansion along the a - and c -axes. For each carbonate the linear thermal expansion along the c -axis is greater than along the a -axis: $\alpha_0(c) = 10.47(11) \times 10^{-5}$ and $8.72(5) \times 10^{-5}$ K⁻¹ and $\alpha_0(a) = 2.84(6) \times 10^{-5}$ and $4.78(5) \times 10^{-5}$ K⁻¹ for $K_2Mg(CO_3)_2$ and $Na_2Mg(CO_3)_2$, respectively. Still, NaMg-double carbonate has a higher relative expansion along the a -axis and a lower one along c in comparison to KMg-double carbonate. Moreover, at atmospheric pressure, $K_2Mg(CO_3)_2$ decomposes between 400 and 450 °C into $MgCO_3$ and a poorly crystalline material, which is 100 °C lower than for $Na_2Mg(CO_3)_2$.

DISCUSSION

Structural behavior of (K,Na)Mg-double carbonates in comparison with dolomite and magnesite

Dolomite and magnesite are dominant in storing oxidized C in the Earth's mantle (e.g., Ross 1997). With increasing pressure, dolomite breaks down to magnesite+aragonite, and it has been demonstrated that the location of this reaction depends on the dolomite composition and ordering effects (Franzolin et al. 2012). Being a double carbonate as the alkali-Mg-bearing carbonates, the dolomite structure is characterized by the presence of alternating $[CaO_6]$ - and $[MgO_6]$ -octahedral layers, intercalated by slightly applanar CO_3^{2-} -groups. The octahedral sites, M1 and M2, are in case of the ordered dolomite ($R\bar{3}$) preferentially occupied by Ca and Mg cations, respectively. Disorder effects take place in dolomite with increasing temperature: Ca and Mg start exchanging between M1 and M2 sites, and above the critical temperature these sites become indistinguishable. The latter is results in a higher symmetry structure ($R\bar{3}c$). Because of the length differences between Ca–O and Mg–O bonds, O-atoms are located closer to Mg than to Ca, causing a rotation of CO_3^{2-} -groups within a given layer around their threefold axis. The angle of rotation was determined as 6.5° (Ross and Reeder 1992; Reeder and Markgraf 1986). In contrast to dolomite, KMg- and NaMg-double carbonates do not show any evidence for a disordering of cations: K or Na and Mg are each hosted exclusively in the $[(K,Na)O_6]$ - and $[MgO_6]$ -coordination polyhedra and their layers, respectively.

With increasing pressure, (K,Na)Mg-double carbonate structures exhibit certain similarities to dolomite and magnesite. Upon compression, metal polyhedra are more compressible than the C–O bonds, which remain almost rigid (Ross 1997; Ross and

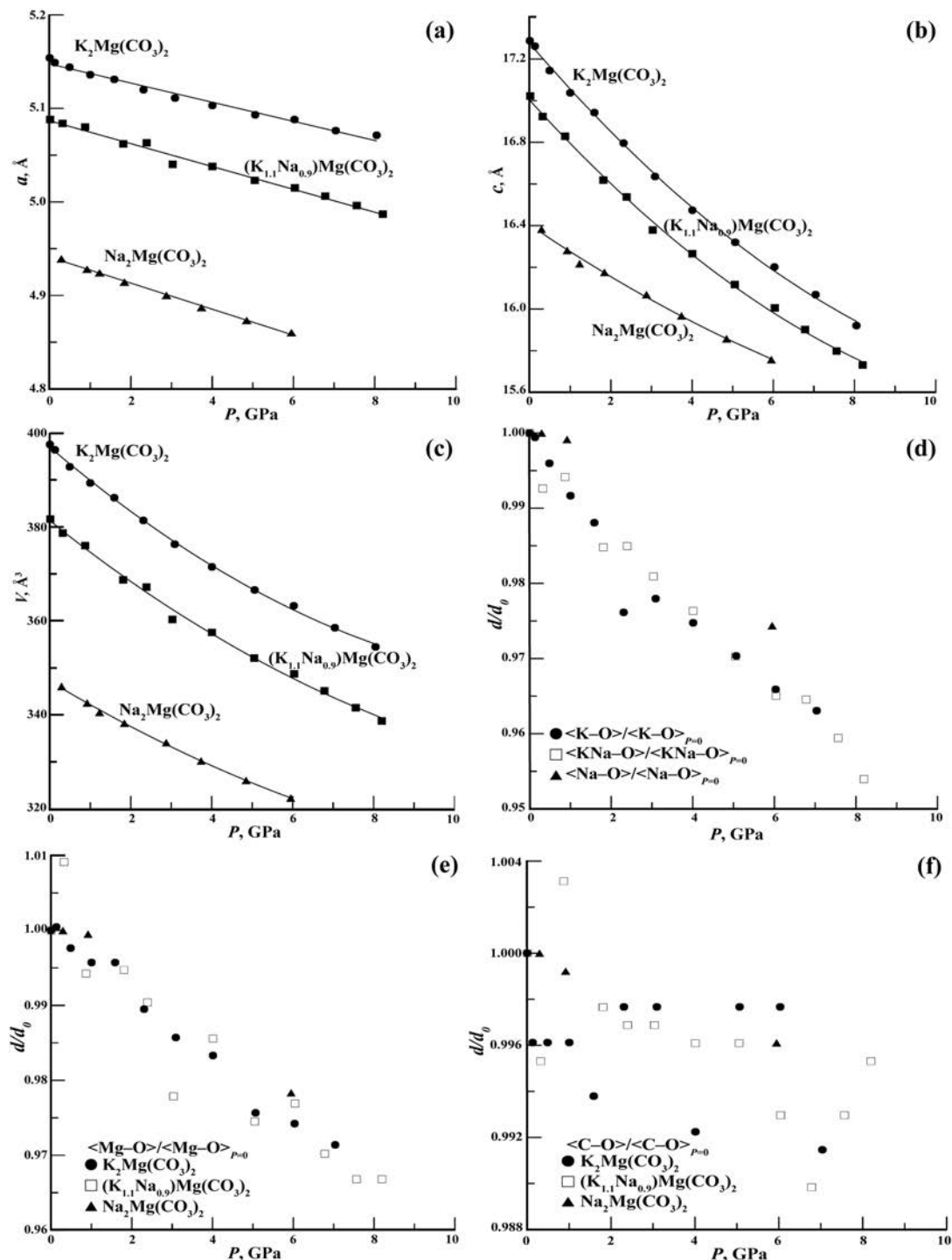


FIGURE 2. Variation of lattice parameters and interatomic distances upon compression. All carbonates are characterized by a higher compressibility along the c - than a -axis and for bonds in $[\text{K}(\text{O}_9)]$ - or $[\text{Na}(\text{O}_9)]$ -polyhedra than in $[\text{Mg}(\text{O}_6)]$ -octahedra. The anisotropy of compression is stronger in KMg - (low- P polymorph) and (K,Na)Mg-double carbonates than in the NaMg -end-member.

Reeder 1992). As in alkali-Mg-double carbonates, in dolomite the polyhedron of the bigger cation, the $[\text{CaO}_6]$ -octahedron, is more compressible than the $[\text{MgO}_6]$ -octahedron. This results in the observed anisotropy of compression along the a - and c -axis, c

being approximately three times more compressible than a (Ross and Reeder 1992). The shortening of alkali metal-O and Ca-O bonds in dolomite and (K,Na)Mg-double carbonates is almost the same and comprises ~3% (to 6 GPa). To 6 GPa Mg-O bonds get

2% shorter with increasing pressure in magnesite, dolomite, and alkali-Mg-double carbonates (Ross 1997; Ross and Reeder 1992).

Dolomite and magnesite transform into high- P polymorphs, dolomite-II and magnesite-II, at 17 and 80 GPa, respectively (Merlini et al. 2012; Boulard et al. 2011), much higher than in $K_2Mg(CO_3)_2$ or $Na_2Mg(CO_3)_2$. $K_2Mg(CO_3)_2$ -II is only 1% denser than $K_2Mg(CO_3)_2$ -I, with a similar density increase as ob-

served in second-order dolomite to dolomite-II transition at 17 GPa (Merlini et al. 2012).

Comparison of densities and bulk moduli

Figure 7 represents a comparison of densities between the (K,Na)Mg-double carbonates and K_2CO_3 , natrite (γ - Na_2CO_3), baylissite [$K_2Mg(CO_3)_2 \cdot 4H_2O$], dolomite, and magnesite (Zubkova et al. 2002; Bucat et al. 1977; Gatehouse and Lloyd 1973). Alkali-alkali earth double carbonates have densities [2.72, 2.73, and 2.80 g/cm³ for $K_{1.1}Na_{0.9}Mg(CO_3)_2$, $Na_2Mg(CO_3)_2$, and $K_2Mg(CO_3)_2$, respectively] which are intermediate between alkali carbonates (2.42 and 2.55 g/cm³ for K_2CO_3 and γ - Na_2CO_3 , respectively) and dolomite and magnesite (2.88 and 2.98 g/cm³ for dolomite and magnesite, respectively). The H_2O -bearing baylissite is characterized by the lowest density (2.05 g/cm³) among the carbonates considered here.

The bulk moduli of K_2CO_3 and Na_2CO_3 are only known from a personal communication with S. Redfern cited by Liu et al. (2007), and amount to 45 and 60 GPa, respectively (Fig. 3). The bulk moduli for the K- and Na-Mg carbonates of 57 and 69 GPa, respectively, are only slightly higher but

TABLE 7. Results of fitting P - V data to the second-order Birch-Murnaghan EoS and V - T data to the formulation of Pawley et al. (1996)

Phase	V_0 (Å ³) ^a	K_0 (GPa)	K'	α_0 ($\times 10^{-5}$ K)
$K_2Mg(CO_3)_2$ -I	396.2(4)	57.0(10)	4	14.31(5)
$K_2Mg(CO_3)_2$ -II	262.6(11)	58.4(20)	4	
$(K_{0.55}Na_{0.45})_2Mg(CO_3)_2$	381.2(5)	54.9(13)	4	
$Na_2Mg(CO_3)_2$	347.1(3)	68.6(13)	4	16.73(11)
$Na_2Mg(CO_3)_2$ (2nd run)	348.6(2)	71.1(4)	4	

^a Recommended values from compression experiments.

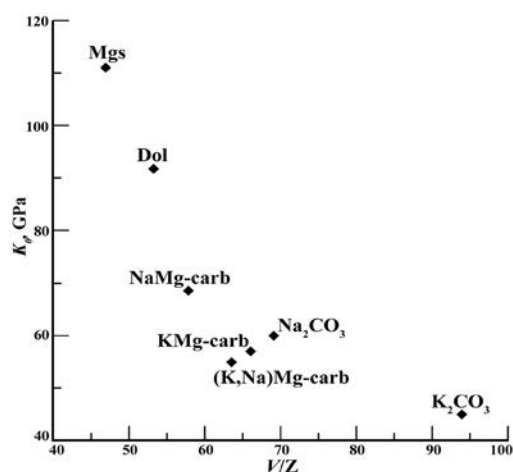


FIGURE 3. Dependence of bulk modulus, K_0 (GPa), on carbonate composition. Carbonates are characterized by an increase in bulk modulus with the substitution of K by Na. For comparison, the bulk moduli of alkali carbonates, magnesite, and dolomite are given (Liu et al. 2007 and references therein; Ross 1997; Ross and Reeder 1992). Mineral abbreviations: Dol = dolomite; KMg-carb = $K_2Mg(CO_3)_2$; (K,Na)Mg-carb = $K_{1.1}Na_{0.9}Mg(CO_3)_2$; Mgs = magnesite; NaMg-carb = $Na_2Mg(CO_3)_2$.

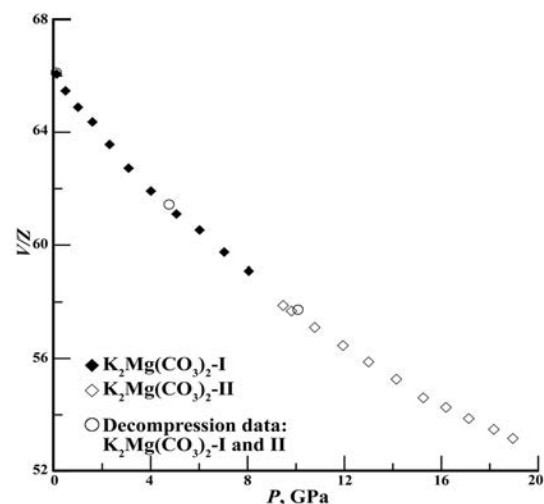


FIGURE 4. Change of volume per formula unit upon compression for the low- and high- P $K_2Mg(CO_3)_2$ polymorphs, $K_2Mg(CO_3)_2$ -I and -II, respectively. Data from the decompression experiments are also shown.

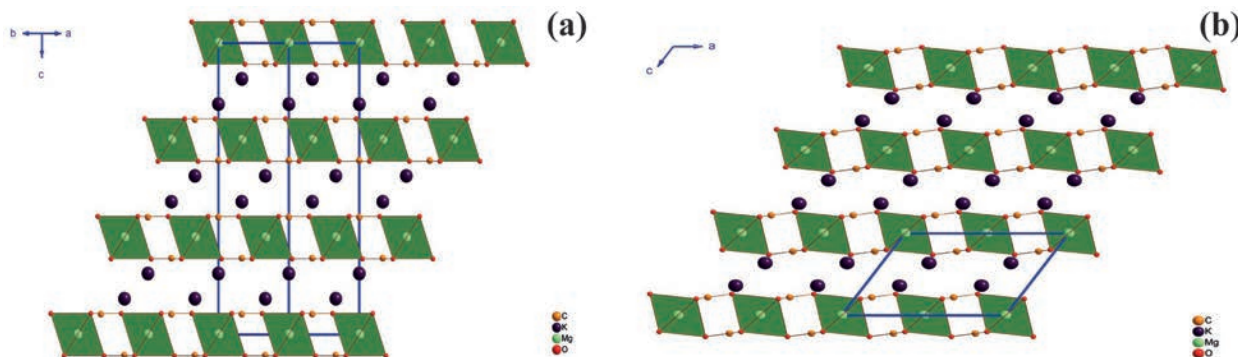


FIGURE 5. Structures of rhombohedral $K_2Mg(CO_3)_2$ -I, viewed along $[110]$ -direction (a), and the monoclinic $K_2Mg(CO_3)_2$ -II, viewed along $[010]$ -direction (b); carbonate groups are tilted in the high-pressure polymorph (b) compared to the low-pressure structure (a).

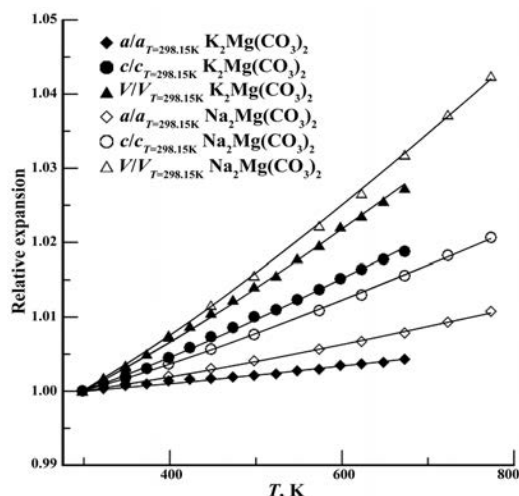


FIGURE 6. Relative expansions of unit-cell parameters (a/a_0 , c/c_0 , V/V_0) with temperature for $K_2Mg(CO_3)_2$ -I and $Na_2Mg(CO_3)_2$. The data were fitted with the expressions for α and V from (Pawley et al. 1996). The NaMg-double carbonate is characterized by a larger increase in volume upon heating (4%) in comparison to the K-bearing end-member (3% volume increase). Both carbonates demonstrate an anisotropy of thermal expansion along the a - and c -axes.

much lower than the values for dolomite (92 GPa) and magnesite (111 GPa) (Ross 1997; Ross and Reeder 1992).

Thermal expansion data

Dobson et al. (1996) reported densities measured for $K_2Mg(CO_3)_2$ at 500 and 564 °C and pointed out that decarbonation prevented the study of KMg-double carbonates over a wider temperature range. In our case decomposition of the KMg-double carbonate took already place between 400 and 450 °C. Nevertheless, our density calculated for $K_2Mg(CO_3)_2$ at 400 °C (2.71 g/cm³) is much higher than the one measured by (Dobson et al. 1996) at 500 °C of 2.26 g/cm³. The latter value is close to the density of baylissite (Bucat et al. 1977) and thus may indicate a sample hydration in the experiments of Dobson et al. (1996).

In comparison to dolomite and magnesite, alkali-alkali earth carbonates have higher coefficients of thermal expansion. When fitted to the T - V EoS of Pawley et al. (1996), the volumetric $\alpha_0 = 7.15(11) \times 10^{-5}$ and $7.7(3) \times 10^{-5}$ K⁻¹ for dolomite and magnesite, respectively (Reeder and Markgraf 1986; Markgraf and Reeder 1985), are lower than $\alpha_0 = 14.31(5) \times 10^{-5}$ and $16.73(11) \times 10^{-5}$ K⁻¹ for KMg- and NaMg-double carbonates, respectively. Magnesite and dolomite are also characterized by an anisotropy of thermal expansion along a - and c -axis: $\alpha_0(a) = 2.02 \times 10^{-5}$ and $1.74(6) \times 10^{-5}$ K⁻¹ and $\alpha_0(c) = 5.08(16) \times 10^{-5}$ and $5.13(7) \times 10^{-5}$ K⁻¹, respectively, and these values are lower than the numbers obtained for $K_2Mg(CO_3)_2$ and $Na_2Mg(CO_3)_2$, i.e., $\alpha_0(a) = 2.84(6) \times 10^{-5}$ and $4.78(5) \times 10^{-5}$ K⁻¹ and $\alpha_0(c) = 10.47(11) \times 10^{-5}$ and $8.72(5) \times 10^{-5}$ K⁻¹, respectively.

High-pressure transformations in (K,Na)Mg-double carbonates: Comparison with published data

Published data on the high-pressure stabilities of $K_2Mg(CO_3)_2$ – $Na_2Mg(CO_3)_2$ are very limited (Shatskiy et al. 2013a,

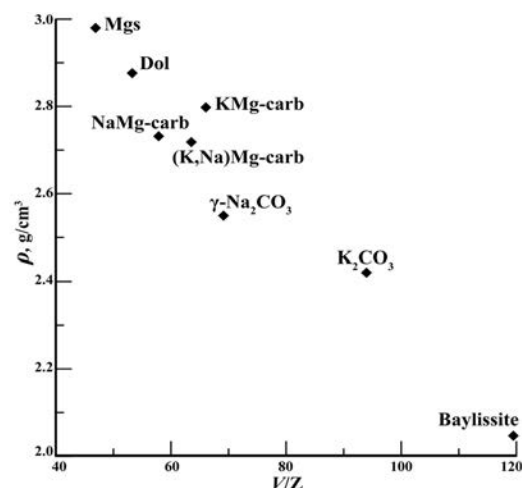


FIGURE 7. Density ρ (g/cm³) of (K,Na)Mg-double carbonates plotted against normalized V (V_0/Z) in comparison with alkali carbonates, baylissite, $K_2Mg(CO_3)_2 \cdot 4H_2O$, magnesite, and dolomite (Zubkova et al. 2002; Bucat et al. 1977; Gatehouse and Lloyd 1973). As in the case of bulk moduli, densities of alkali-alkali earth carbonates are intermediate between alkali carbonates and magnesite.

2013b). Nevertheless, the change of structure of $K_2Mg(CO_3)_2$ upon compression concurs with the experimental study of Shatskiy et al. (2013), where a phase transition to a possibly orthorhombic polymorph at 6.5 GPa and 1000 °C was proposed based on the analysis of diffraction patterns for K-Mg-carbonate mixture. The indexing attempt of this high P - T polymorph (Shatskiy et al. 2013) provides a unit-cell volume indicating a 10% density increase on transition if compared to our equation of state. The reported density increase is comparable, for example, to the density change in magnesite to magnesite-II (Boulard et al. 2011) at 80 GPa, where a completely new topology is observed, based on tetrahedral CO_4 groups. It is unlikely that at the much lower pressures investigated by (Shatskiy et al. 2013) a major structural change is established, and probably the density is overestimated. Moreover, in the absence of a structure determination, any indexing of a powder pattern should be considered with caution. The actual lattice and structure of the high P - T polymorph, therefore, must still be addressed. Nevertheless, combining both our and the Shatskiy et al. (2013) results, a limit of pressure and temperature stability for the rhombohedral $K_2Mg(CO_3)_2$ $R\bar{3}m$ structure of 8.2 GPa at 25 °C and 6.5 GPa at 1000 °C, yields a slightly negative Clapeyron slope. The Na-end-member did show a transformation to a high-pressure polymorph at 13.6 GPa, ambient temperature but none to 6 GPa at high temperature.

IMPLICATIONS

(K,Na)Mg-double carbonates may play an important role in mantle processes, by the lowering of melting temperatures of mantle peridotites. Therefore, in the present work we analyzed the structural behavior of three different carbonates on the $K_2Mg(CO_3)_2$ – $Na_2Mg(CO_3)_2$ join upon compression. The bulk modulus of the carbonates investigated is between 55 and 70 GPa, with higher values for the $Na_2Mg(CO_3)_2$ end-member. We notice

that $\text{K}_2\text{Mg}(\text{CO}_3)_2$ and $\text{K}_{1.1}\text{Na}_{0.9}\text{Mg}(\text{CO}_3)_2$ exhibit very similar values, while eitelite has a lower compressibility. $\text{Na}_2\text{Mg}(\text{CO}_3)_2$ crystallizes in the $R\bar{3}$ space group, compared to $R\bar{3}m$ symmetry of the K-bearing compositions. The distorted NaO_9 -polyhedron is in fact less flexible and compressible than the larger and more symmetric KO_9 -coordination site.

In terms of expected occurrence in nature, the K-rich double carbonate has a smaller unit-cell volume and higher density than K_2CO_3 and magnesite combined, while the contrary is true for the NaMg double carbonate. Hence, $\text{K}_2\text{Mg}(\text{CO}_3)_2$ may well occur in nature at mantle pressures and is in fact observed in high-pressure experiments at 7 GPa (Golubkova and Schmidt 2015). Eitelite, $\text{Na}_2\text{Mg}(\text{CO}_3)_2$, should be disfavored by high pressures and is in fact observed in Na-carbonatites.

ACKNOWLEDGMENTS

ESRF synchrotron facility is acknowledged for high-pressure measurements at ID09A beamline. Elettra synchrotron facility is acknowledged for high temperature measurements at MCX beamline. M. Hanfland, A. Lausi, J. Plaiser, and M. Abdellatif are acknowledged for assistance during synchrotron experiments.

REFERENCES CITED

- Anthony, J.W., Bideux, R.A., Bladh, K.W., and Nichols, M.C. (1997) Handbook of Mineralogy, vol. V—Borates, Carbonates, Sulfates. Mineral Data Publishing, Tucson, Arizona.
- Angel, R.J. (2000) Equations of State. Mineralogical Society of America and The Geochemical Society, Chantilly, Virginia.
- Artemieva, I.M. (2009) The continental lithosphere: Reconciling thermal, seismic, and petrologic data. *Lithos*, 109, 23–46.
- Boulard, E., Gloter, A., Corgne, A., Antonangeli, D., Auzende, A.L., Perrillat, J.P., Guyot, F., and Fiquet, G. (2011) New host for carbon in the deep Earth. *Proceedings of the National Academy of Sciences*, 108, 5184–5187.
- Brey, G.P., Bulatov, V.K., Girmis, A.V., and Lahaye, Y. (2008) Experimental melting of carbonated peridotite at 610 GPa. *Journal of Petrology*, 49, 797–821.
- Brey, G.P., Bulatov, V.K., and Girmis, A.V. (2011) Melting of K-rich carbonated peridotite at 6–10 GPa and the stability of K-phases in the upper mantle. *Chemical Geology*, 281, 333–342.
- Bucat, R.B., Patrick, J.M., White, A.H., and Willis, A.C. (1977) Crystal structure of baylissite, $\text{K}_2\text{Mg}(\text{CO}_3)_2 \cdot 4\text{H}_2\text{O}$. *Australian Journal of Chemistry*, 30, 1379–1382.
- Dawson, J.B. (1962a) The geology of Oldoinyo Lengai. *Bulletin of Volcanology*, 24, 349–387.
- (1962b) Sodium carbonate lavas from Oldoinyo Lengai. *Nature*, 195, 1075–1076.
- Dobson, D.P., Jones, A.P., Rabe, R., Sekine, T., Kurita, K., Taniguchi, T., Kondo, T., Kato, T., Shimomura, O., and Urakawa, S. (1996) In-situ measurement of viscosity and density of carbonate melts at high pressure. *Earth and Planetary Science Letters*, 143, 207–215.
- Franzolin, E., Merlini, M., Poli, S., and Schmidt, M.W. (2012) The temperature and compositional dependence of disordering in Fe-bearing dolomites. *American Mineralogist*, 97, 1676–1684.
- Frost, D.J., and McCammon, C.A. (2008) The redox state of Earth's mantle. *Annual Review of Earth and Planetary Sciences*, 38, 49–70.
- Gaines, R.V., Skinner, H.C.W., Foord, E.E., and Rosenzweig, A. (1997) Dana's New Mineralogy: Eighth edition. Wiley, New York.
- Gasparik, T., and Litvin, Y.A. (2002) Experimental investigation of the effect of metasomatism by carbonic melt on the composition and structure of the deep mantle. *Lithos*, 60, 129–143.
- Gatehouse, B.M., and Lloyd, D.J. (1973) Crystal structure of anhydrous potassium carbonate. *Journal of the Chemical Society-Dalton Transactions*, 70–72.
- Ghosh, S., Ohtani, E., Litasov, K.D., and Terasaki, H. (2009) Solidus of carbonated peridotite from 10 to 20 GPa and origin of magnesite-carbonatite melt in the Earth's deep mantle. *Chemical Geology*, 262, 17–28.
- Giuliani, A., Kamenetsky, V.S., Phillips, D., Kendrick, M.A., Wyatt, B.A., and Goemann, K. (2012) Nature of alkali-carbonate fluids in the sub-continental lithospheric mantle. *Geology*, 40, 967–970.
- Golubkova, A., and Schmidt, M.W. (2015) Slab-derived carbonate melts reacting in the mantle and kimberlite source region metasomatism. *Journal of Petrology*, in press.
- Grassi, D., and Schmidt, M.W. (2011a) Melting of carbonated pelites at 8–13 GPa: Generating K-rich carbonatites for mantle metasomatism. *Contributions to Mineralogy and Petrology*, 162, 169–191.
- (2011b) The melting of carbonated pelites from 70 to 700 km depth. *Journal of Petrology*, 52, 765–789.
- Hesse, K.-F., and Simons, B. (1982) Crystal structure of synthetic $\text{K}_2\text{Mg}(\text{CO}_3)_2$. *Zeitschrift für Kristallographie*, 161, 289–292.
- Hirschmann, M.M. (2000) Mantle solidus: Experimental constraints and the effects of peridotite composition. *Geochemistry Geophysics Geosystems*, 1, 1042–1067.
- Holland, T.J.B., and Powell, R. (1998) An internally consistent thermodynamic data set for phases of petrological interest. *Journal of Metamorphic Geology*, 16, 309–343.
- Klein-BenDavid, O., Logvinova, A.M., Schrauder, M., Spetius, Z.V., Weiss, Y., Hauri, E.H., Kaminsky, F.V., Sobolev, N.V., and Navon, O. (2009) High-Mg carbonatitic microinclusions in some Yakutian diamonds—A new type of diamond-forming fluid. *Lithos*, 112, 648–659.
- Larson, A.C., and Von Dreele, R.B. (1994) General structure analysis system (GSAS). Los Alamos National Laboratory Report LAUR 86-748.
- Liu, Q., Tenner, T.J., and Lange, R.A. (2007) Do carbonate liquids become denser than silicate liquids at pressure? Constraints from the fusion curve of K_2CO_3 to 3.2 GPa. *Contributions to Mineralogy and Petrology*, 153, 55–66.
- Markgraf, S.A., and Reeder, R.J. (1985) High-temperature structure refinements of calcite and magnesite. *American Mineralogist*, 70, 590–600.
- McKie, D., and Frankis, E.J. (1977) Nyereite: A new volcanic carbonate mineral from Oldoinyo Lengai, Tanzania. *Zeitschrift für Kristallographie*, 145, 73–95.
- Merlini, M., and Hanfland, M. (2013) Single-crystal diffraction at megabar conditions by synchrotron radiation. *High Pressure Research*, 33, 511–522.
- Merlini, M., Crichton, W.A., Hanfland, M., Gemmi, M., Müller, H., Kuzenko, I., and Dubrovinsky, L. (2012) Structures of dolomite at ultrahigh pressure and their influence on the deep carbon cycle. *Proceedings of the National Academy of Sciences*, 109, 13,509–13,514.
- Oszlanyi, G., and Suto, A. (2007) Ab initio neutron crystallography by the charge flipping method. *Acta Crystallographica*, A63, 156–163.
- Pabst, A. (1973) Crystallography and structure of eitelite, $\text{Na}_2\text{Mg}(\text{CO}_3)_2$. *American Mineralogist*, 58, 211–217.
- (1974) Synthesis, properties, and structure of $\text{K}_2\text{Ca}(\text{CO}_3)_2$, buetschliite. *American Mineralogist*, 59, 353–358.
- Palatinus, L., and Chapuis, G. (2007) SUPERFLIP—A computer program for the solution of crystal structures by charge flipping in arbitrary dimensions. *Journal of Applied Crystallography*, 40, 786–790.
- Palme, H., and O'Neill, H.St.C. (2003) Cosmochemical estimates of mantle composition. Elsevier, Amsterdam.
- Pawley, A.R., Redfern, S.A.T., and Holland, T.J.B. (1996) Volume behavior of hydrous minerals at high pressure and temperature. I. Thermal expansion of lawsonite, zoisite, clinozoisite, and diaspore. *American Mineralogist*, 81, 335–340.
- Pertlik, F. (1981) Structural investigations of synthetic fairchildite, $\text{K}_2\text{Ca}(\text{CO}_3)_2$. *Zeitschrift für Kristallographie*, 157, 199–205.
- Petríček, V., Dušek, M., and Palatinus, L. (2014) Crystallographic Computing System JANA2006: General features. *Zeitschrift für Kristallographie*, 229, 345–352.
- Pollack, H.N., and Chapman, D.S. (1977) Regional variation of heat-flow, geotherms, and lithospheric thickness. *Tectonophysics*, 38, 279–296.
- Reeder, R.J., and Markgraf, S.A. (1986) High-temperature crystal chemistry of dolomite. *American Mineralogist*, 71, 795–804.
- Riello, P., Lausi, A., Macleod, J., Plaisier, J.R., Zerauscheck, G., and Fornasiero, P. (2013) In situ reaction furnace for real-time XRD studies. *Journal of Synchrotron Radiation*, 20, 194–196.
- Ross, N.L. (1997) The equation of state and high-pressure behavior of magnesite. *American Mineralogist*, 82, 682–688.
- Ross, N.L., and Reeder, R.J. (1992) High-pressure structural study of dolomite and ankerite. *American Mineralogist*, 77, 412–421.
- Shatskiy, A., Gavryushkin, P.N., Sharygin, I.S., Litasov, K.D., Kupriyanov, I.N., Higo, Y., Borzdov, Y.M., Funakoshi, K.I., Polyakov, Y.N., and Ohtani, E. (2013a) Melting and subsolidus phase relations in the system $\text{Na}_2\text{CO}_3\text{--MgCO}_3\text{--H}_2\text{O}$ at 6 GPa and the stability of $\text{Na}_2\text{Mg}(\text{CO}_3)_2$ in the upper mantle. *American Mineralogist*, 98, 2172–2182.
- Shatskiy, A., Sharygin, I.S., Gavryushkin, P.N., Litasov, K.D., Borzdov, Y.M., Shcherbakova, A.V., Higo, Y., Funakoshi, K.-i., Polyakov, Y.N., and Ohtani, E. (2013b) The system $\text{K}_2\text{CO}_3\text{--MgCO}_3$ at 6 GPa and 900–1450 °C. *American Mineralogist*, 98, 1593–1603.
- Toby, B.H. (2001) EXPGUI, a graphical user interface for GSAS. *Journal of Applied Crystallography*, 34, 210–213.
- Winbo, C., Bostrom D., and Gobbels M. (1997) Crystal structure of the double carbonate $\text{K}_2\text{Ca}_2(\text{CO}_3)_3$. *Acta chemica Scandinavica*, 51, 387–391.
- Zedgenizov, D.A., Ragozin, A.L., Shatsky, V.S., Araujo, D., Griffin, W.L., and Kagi, H. (2009) Mg and Fe-rich carbonate-silicate high-density fluids in cuboid diamonds from the International kimberlite pipe (Yakutia). *Lithos*, 112, 638–647.
- Zubkova, N.V., Pushcharovsky, D.Y., Ivaldi, G., Ferraris, G., Pekov, I.V., and Chukanov, N.V. (2002) Crystal structure of natrite, gamma- Na_2CO_3 . *Neues Jahrbuch für Mineralogie-Monatshefte*, 85–96.

MANUSCRIPT RECEIVED OCTOBER 9, 2014

MANUSCRIPT ACCEPTED APRIL 25, 2015

MANUSCRIPT HANDLED BY LARS EHM